SLAC–PUB–6572
January 1995
(A)

X-Ray Photoelectron Spectroscopy Study of the Difference between Reactively Evaporated and Direct Sputter–Deposited TiN Films and Their Oxidation Properties[◊]

P. PRIETO* AND R. E. KIRBY

Stanford Linear Accelerator Center,
Stanford University, Stanford, California 94309

Journal of Vacuum Science and Technology A

[◊]Work supported in part by US Department of Energy contract DE–AC03–76SF00515 (SLAC) and by the Spanish Ministry of Education and Science.

*Current Address: Departamento Fisica Aplicada C-XII, Universidad Autonoma Madrid, Cantoblanco 28049 Madrid, Spain.

ABSTRACT

X-ray photoelectron spectroscopy (XPS) technique has been used to study carefully prepared oxide-free titanium nitride (TiN) films of nearly identical stoichiometry, grown by direct sputtering and reactive evaporation. The lineshapes and peak positions of the Ti 2p and N 1s transitions are dependent upon the deposition method. The XPS results showed that oxynitrides are present following exposure of either type of film to dry oxygen; however, reactively evaporated films have a considerably higher oxidation rate. Differences in valence band and electron energy loss spectroscopy (EELS) spectra are correlated with the changes observed in the core levels. The EELS spectra detected the presence of a low energy loss, which is correlated with the TiN electron density of states closest to the Fermi level. The secondary electron emission yields for reactively evaporated TiN were also measured before and after dry oxygen and air exposure, and after heating.

INTRODUCTION

The TiN coatings are used very successfully in a variety of applications (such as hard metallurgical coatings and diffusion barriers in semiconductor technology) because of their thermodynamic stability and low electrical resistivity [1]. These coatings are of interest because they exhibit a number of properties similar to metals (such as good electrical conductivity and superconductivity) while retaining characteristics (covalent bonds, hardness, brittleness, and a high melting point) found in insulating materials [2]. It is known that these properties of TiN films depend strongly on deposition parameters [3].TiN is also interesting from a more fundamental point of view—particularly interesting is the relation between its macroscopic properties and electronic structure. The valence band electronic structure of TiN has been studied before—both theoretically [4-5] and experimentally [6-10]—suggesting that the valence electrons are responsible for the mixture of covalent and ionic bonds in this material, which results in a combination of metallic and insulating properties.

TiN coatings are also used to suppress secondary electron emission in particle accelerator structures and storage ring components [11,12], where it is useful in both rf (thin, low power-loss film) and dc (thick film) cases. A variety of TiN deposition geometries have been used at the Stanford Linear Accelerator Center depending on the shape requirements of the components, sometimes incorporating reactive sublimation of Ti in a N_2 atmosphere, and

often using dc sputtering from a TiN target or reactive sputtering in a N_2 atmosphere. Film stoichiometries from these various methods have been similar but resistance to oxidation has never been determined, although this is an important consideration for components routinely exposed to air prior to final assembly.

The literature contains a number of photoelectron spectroscopic studies of TiN [9,13-16] and oxidized TiN [11,17-22], but the information presented is often conflicting or incomplete from the point of view of characterization of both the spectra and the material composition. The natural shape of Ti 2p transition is complex; in some cases, it shows features at the higher binding energy sides of both the Ti $2p_{3/2}$ and Ti $2p_{1/2}$ transitions. These features fall in the binding energy range of TiO_xN_y compounds, thus complicating interpretation.

Our intent is to clarify the origin of the different components that comprise the Ti 2p, N 1s and O 1s levels in both clean and oxidized TiN, and their dependence upon the fabrication method. We have also measured electron energy loss spectroscopy (EELS) and valence band spectra to observe the changes induced in the electronic structure.

EXPERIMENTAL

The 14 nm-thick TiN films of near-stoichiometric composition were grown by two different methods: reactive evaporation (hereafter designated "re") in a nitrogen atmosphere of varying

pressure (5×10^{-4} to 5×10^{-6} Torr), and by direct sputtering from a TiN target (designated "sp"). The substrates used in this work were stainless steel, sputter-cleaned *in situ*. Deposition thicknesses were determined by a quartz-crystal thickness monitor. The sp films were produced using a Kaufman-type ion source bombarding a 99.9% pure compacted powder TiN target at an Ar pressure of 7×10^{-5} Torr and 1500 eV ion energy. The thickness chosen was sufficient to prevent substrate effects from contributing to the x-ray photoelectron spectroscopy (XPS) and Auger electron spectroscopy (AES) intensities (escape depths < 5 nm). However, this is also a typical thickness used in coating SLAC accelerator components.

The characterization of both types of films was done *in situ*, following deposition. This is particularly important because air exposure of TiN produces an oxidized layer that compromises surface characterization of as-deposited surfaces. In such cases of air exposure, ion bombardment has been used typically to remove the oxide, but such a procedure produces chemical reduction, atomic mixing, preferential sputtering, and other effects that modify the surface.

Surface analytical spectra were acquired with a Vacuum Generators, Ltd. Model CLAM 100 x-ray photoelectron spectroscopy unit. Pressure was typically 5×10^{-11} Torr in the analysis chamber and 3×10^{-10} Torr in the film deposition chamber.

A magnetically-coupled motion transfer system connected the two chambers, allowing the beginning of analysis to occur within 30 minutes of film deposition. The XPS data were collected using Mg K_α radiation, with the analyzer operating in the constant analyzer pass energy mode, with total instrumental resolution < 0.75 eV FWHM. Photoelectrons were collected from a 4×4 mm^2 sample area, 15° from surface normal. Binding energy (BE) references for XPS are the Pd Fermi edge (BE=0) and the Ag $3d_{3/2}$ core line (BE=368.2 eV). In both kinds of samples, we have measured XPS Ti 2p, N 1s and O 1s spectra—50 eV BE of valence band spectra, including Ti 3p, N 2s, and O 2s, were also acquired. Secondary electron emission yields were measured by retarding potential [12] with a 1.0 keV, 2 nA electron beam, EELS spectra were acquired at 300 eV primary energy, with the incident beam 19.5° from normal incidence.

The TiN samples were oxidized by exposure to dry oxygen at 10^{-2} Torr and one atmosphere at room temperature for up to 100 minutes in order to study the nature of the oxide layer in the two different titanium nitrides. Some surface modification studies were carried out by heating (825 and 1100 K) and by 500 eV ion bombardment. Spectra were fitted using a least-squares method with a Gaussian/Lorentzian (G/L) peak shape with a 50% G/L mixing ratio for symmetrical spectra (N 1s, O 1s, and Ti 2p oxide).

The asymmetrical lineshapes found in Ti 2p metal and nitride were well fitted with Doniach–Sunjic functions.

DISCUSSION

Clean Titanium Nitride

The XPS spectra of the Ti 2p and N 1s core levels for titanium nitride produced by sp and by re are shown in Figs. 1(a) and (b), respectively. The composition of these samples, obtained by correcting for XPS intensities (sensitivity factors S(Ti)=2.04, S(N)=0.49, and S(O)=0.72) for this type of spectrometer [23], produced a surprising result: the composition in both cases was $TiN_{0.9}$, but the corresponding Ti 2p lineshape in the samples is clearly different (see Fig. 1). We confirmed the results of the composition calculation using both the AES quantification method of Dawson and Tzatzov [24] and that of Sungred [25], which both involve separating the overlapping transitions N($KL_{2,3}L_{2,3}$) and Ti ($L_{2,3}M_{2,3}M_{2,3}$) into N and Ti components. No evidence of oxygen was detectable in the XPS or AES data of the as-deposited TiN layers.

The sp Ti 2p doublet in Fig. 1(a) (solid line) clearly shows an asymmetry, and is well fitted with Doniach–Sunjic (D–S) functions (dotted lines), convoluted with our analyzer's resolution function (FWHM=0.3 eV) and MgK_α x-ray lineshape. D–S lines were also previously used for the fit of the Ti 2p doublet of metallic

titanium, in agreement with the good electrical conductivity of both Ti and TiN. D–S lines exhibit exponential tails closely related to the coupling of the core holes with conduction electrons at the Fermi level. The parameters of the Ti $2p_{3/2}$ D–S line are 1.10, 0.41, and 0.32 for the Gaussian width, Lorentzian width, and asymmetry, respectively. However, the re Ti 2p doublet, Fig. 1(b) (solid line), is not well fitted with only D–S functions, and is clearly formed from more than a single component pair. The difference spectrum (Ti 2p sp –Ti 2p re) is shown in Fig. 1(b) (open circles), and is fitted with a pair of Gaussian "satellites" at 1.7 eV higher binding energy (BE) than the corresponding D–S lines.

The Ti 2p and N 1s fitting parameters for both sample types are listed in Table I. In sp TiN, the BE shift between the nitride and metal for Ti 2p level was 0.7 eV, but it was 1.1 eV in re TiN. The binding energies for the N 1s are weakly different: 397.1 eV (sp) and 396.9 eV (re). The large BE width of N 1s line in the re case (1.65 eV compared to 1.20 eV for sp TiN) suggests a disordered or defective structure. The apparent binding energy difference (ABE) between Ti $2p_{3/2}$ and N 1s contains information about ligand charge transfer because it is not affected by the BE reference level, and the relaxation energies for Ti and N core holes should be similar. For sp, TiN ABE = 57.6 eV, while for re, TiN = 58.2 eV. This is a clear indication that the charge transfer in re TiN is larger than in sp, and is not due to a nitrogen composition difference.

We found that the shape and the peak positions of the Ti 2p and N 1s transitions are strongly dependent upon the film deposition method, but for re films, apparently not dependent on nitrogen composition. A nitrogen pressure of 5×10^{-4} Torr produced a composition of $TiN_{0.9}$. Varying the pressure between 5×10^{-5} and 5×10^{-6} Torr produces a composition of $TiN_{1.1}$. The lineshape in all cases was as shown in Fig.1(b), with an unchanged relative ratio of satellite-to-main-line intensity uncorrelated to nitrogen pressure. Takeoff angle experiments on the re films indicated that the satellite structure of Fig.1(b) is not due to a small surface contamination (as monitored at the C1s and O1s BE regions of the spectrum). The principle difference among the Ti 2p spectra at different takeoff angles was in the background levels caused by inelastic scattering of the photoelectrons; however, the intensity relationship of the satellite and main lines remained constant. This means that the satellite structure is not caused by compositional differences or surface effects, but is probably due to a structural difference.

There are interpretational differences in the literature about the natural lineshape of the Ti 2p in TiN. Burrow et al [26] and Porte et al [9] found a satellite structure which depends on nitrogen content. In addition, Burrow et al [26] found no correlation of this feature with the oxygen content of the film, while Porte argued against the presence of oxides of titanium as the cause of this feature, on the basis that surface oxides should be detectable at

459 eV, as TiO_2. Other authors (e.g., Robinson et al [18] and C. Ernsberger [20]) have argued for the presence of an oxynitride peak at the same BE position as the satellite, while Saha et al [22] connected the satellite to grain boundaries between TiN and TiO_2 in oxidized TiN. We have not detected oxygen in either sp or re samples by XPS or AES, and therefore believe that our satellite is a natural feature of TiN or its preparation method.

The principal non-oxygen interpretations concerning the source of the satellite structure are:

(1) Ti 3d electron screening of the core hole created during the photoemission process decreases discontinuously with increasing N content [9]. The probability of core-hole screening drops dramatically, with a corresponding increase in the intensity of the unscreened final-state satellite.

(2) "Shakeup" structure due to a loss energy of few eV caused by an intraband transition (t_{1g} to $2t_{2g}$) between occupied and unoccupied electron states near the Fermi level. The authors of this interpretation [27] made a correlation between this structure and a low energy plasmon in the EELS spectra but we think that this is not the solution because the plasmon appears in other transition metals not possessing a satellite structure (Zr and Nb) [28] and also in the EELS spectra of both kinds of TiN samples (as we shall see later in Fig. 7), one of which has no satellite structure.

The first interpretation is a likely fit to our data, but due to a structural effect, rather than changing N content. In re TiN, the N 1s FWHM and the Ti $2p_{3/2}$–N 1s separation is larger than in sp TiN due to a structural difference between re and sp films. Valence band results (also presented below) show evidence of increased ionicity in re TiN. We observed an increased sheet resistance of re TiN over sp films, typical of structural disorder affecting the conductivity. Because the stoichiometry is identical for the two types of films and the satellite structure appears in re films at different nitrogen compositions, the disorder is unlikely to be N vacancies. For the sake of completeness, we have observed the energy-broadened satellite structure in the re Ti 3p as well as 2p levels.

Heating treatment and Ar ion bombardment effect

Both kinds of samples have been bombarded with Ar^+ ions of 500 eV energy, resulting in the reduction of nitrogen content in both cases. Figure 2 shows the Ti 2p and N 1s levels after Ar^+ bombardment of re TiN at angles of 15° and 60° from the surface normal. At the higher angle the composition decreases more rapidly due to nitrogen preferential sputtering in the extreme surface layer, but the more interesting effect was that the satellite structure essentially disappeared at either angle and the width of N 1s level decreased, shifting this line up in BE 0.2 eV. This effect also occurred when re TiN was heated to 1100 K for 5 minutes,

while heating at 825 K was not sufficient to produce any significant change in the as-deposited re film.

Ion-bombardment is normally expected to introduce N vacancies, as is probably the case here; however, that process is unrelated to the cause of the satellite structure as we have observed in the previous section. The energy delivered to the re layer by either ions or thermally does, however, modify the structure and remove the cause of the satellite.

Oxidation

The TiN surfaces produced by re and sp were exposed to dry oxygen at $P_{O_2}=1\times10^{-2}$ Torr and room temperature under the following circumstances: both types as deposited, and re films that were post-deposition bombarded by 500 eV Ar^+ ions prior to oxygen exposure. A virgin re film was also exposed to air in order to compare the oxide thickness and species with those observed under dry oxygen exposure. Air oxidation of sp TiN has been study previously [12]. Because of our interest in the use of TiN as an accelerator component coating, the secondary electron emission yield was also measured on the various oxidized surfaces.

The XPS results for sp TiN after 6.6×10^7 L dry oxygen exposure are presented in Fig. 3 after background subtraction by standard procedures [29,30]. This results in oxidation saturation because we get an identical result at shorter exposures with the same

oxygen pressure. In order to determine the oxidized species, the Ti 2p spectrum corresponding to clean bulk TiN was subtracted from the oxidized data (solid line) and is shown in Fig. 3(a) (dashed). Least square fitting of the oxidized spectrum (vertical scale expanded) is shown in Fig. 3(b). The binding energies of the two set of peaks that appear in the oxidized spectrum are energy-shifted 1.50 and 3.70 eV from Ti metal. The expected shift for TiO_2 is 4.9 eV, so neither of these species corresponds to TiO_2. Supporting this conclusion, the ABE between Ti 2p and O1s ranges between 74.00 and 76.20 eV, compared to 71.5 eV expected for TiO_2 [11]. On other hand, analysis of the N1s spectrum shows [Fig. 3(c)] shows a major component at 397.1 eV due to nitride and a small contribution (shaded peak) shifted to 0.95 eV lower BE and associated with the oxidized species in the Ti 2p spectrum.

Figure 4 presents the Ti 2p, N1s and O1s levels for re films after 6.6×10^{-7} L dry oxygen exposure [Fig. 4(b)]. The spectra obtained after heating the oxidized film at 825 K for 8 hours is also included [Fig. 4(c)]. Comparing the spectra after oxidation for both types of samples [Fig. 3(a) and Fig. 4(b)], we can conclude that re films are more reactive to oxidation because the intensity at higher binding energies associated with the oxidized films is higher than in the sp samples. We have done the same fitting analysis as for previous films. The spectrum of the Ti 2p oxidized species obtained after subtraction of the clean re Ti 2p spectrum is depicted in

Fig. 4(b)by a dashed line. Contrary to the results found in the oxidation of sp layers, the difference spectrum contains only one peak, at 457.05 eV. Furthermore, the N 1s line is comprised of two major components, one of which is at the same binding energy as the nitride and the other is shifted 1.00 eV to lower BE (shaded peak).

The species that appear in the oxidation of TiN have drawn a variety of interpretations in the literature [17–21,31–33]. At oxidation temperatures higher than 400°C, only TiO_2 is found in the oxidized layer [31]. At room temperature, some authors [21] have also found that the oxidized layer is formed by TiO_2. Ermolieff et al [32] have proposed an oxidation of suboxides at the interface between the oxide and the nitride. Robinson et al [18] found that TiN films are oxidized to TiO_2 with a sublayer of oxynitrides, while Ernesberger et al [19,20] label oxynitrides as the principal species resulting from TiN oxidation, with the Ti 2p BE peak laying between the nitride and oxide. More recently, oxide and oxynitride contributions were proposed for the oxidation of ZrN [33]. Conversely, all authors assign N 1s BE peaks above the nitride to an oxynitride, e.g., 399.3 eV to $TiN_{0.5}O_{0.5}$ [17] and 398.4–399.9 eV to "oxynitride" [18]. Peaks whose BE are below the nitride (1 eV or so) are associated with substoichiometric nitrides. However, the N 1s line for substoichiometric zirconium nitrides appears around the binding energy of the stoichiometric nitride [34], while in the

oxidation of ZrN [33], an oxynitride contribution in the N1s line was found at 396.2 eV shifted 1.1 eV from the nitride (BE = 397.3 eV).

We find no TiO_2 contributions in our oxidized spectra of either re or sp films; therefore, the oxidized species are presumably oxynitrides. These are the N1s at 395.9-396.1 eV and Ti$2p_{3/2}$ in the 455.5–457.7 eV BE range. A result of this is opposite BE shifts for the Ti and N lines. The Ti$2p_{3/2}$–N1s ABE changes from 58.2 and 57.6 eV for the re and sp as-deposited nitrides to 60.15 and 59.4-61.6 eV for the corresponding oxynitrides. This is a clear indication of the charge transfer from Ti to N in the oxynitride caused by the increasingly ionic-like character of the bonding.

The annealed oxidized spectra of re films [Fig. 4(c)] show significant differences in shape and position with respect to the as-oxidized layer [Fig. 4(b)]. In the Ti2p level, the oxynitride peak at 457.05 eV declines and is replaced with a line at 458.2 eV. In this case, the ABE in the Ti 2p level between the oxidized species and the metal is 4.2 eV closer to the value for TiO_2 (4.9 eV). The N1s oxynitride contribution at 395.9 eV is exchanged for a major component at 397.0 eV (i.e., BE of the nitride). Furthermore, the O1s level appears at 530.5 eV shifted 0.7 eV to higher BE, which is the literature value for TiO_2 (530.5 eV [35,36]). In conclusion, after annealing at 825 K, the oxynitride components disappear and there appears to be a phase separation into TiN and TiO_2.

A more quantitative insight into the composition and thickness of the oxidized layer can be obtained if some model is assumed for the overlayer. The simplest is that of a TiN substrate covered by an oxynitride layer, TiN_xO_y. Initially, we also tried a model where a TiN substrate was covered by an oxynitride layer and a second layer of TiO_2, but poor results were obtained. Using the TiN_xO_y-only model, the average composition and thickness of the oxidized layer are estimated in terms of the intensities of the individual signals. The general expressions are well known and have been given in detail in Ref. [37]. The thickness of the oxidized layer in sp films was 0.81 nm and the composition was $TiN_{0.9}O_{0.7}$, while the oxidation of re films formed an oxidized layer of $TiN_{0.7}O_{0.9}$ composition and 2.35 nm thick. After 825 K annealing of the oxidized re films, the thickness of the oxidized layer decreased to 0.6 nm. These results show that TiN is more reactive to oxidation than sp TiN, but both types of oxidized layers formed oxynitrides whose composition depends of the fabrication method. The differences found in the oxidation of both kinds of samples are in line with the structural differences previously proposed. Sputter-deposited TiN films are probably denser than reactively evaporated films.

In a separate oxidation experiment, both kinds of films were bombarded with 0.5 keV Ar^+ ions before dry oxygen exposure. In sp films the results are similar to those obtained without Ar^+

bombardment. However, for re films the results are different. In Fig. 5(a) is shown the oxidation, with 6.6×10^7 L dry oxygen, of previously bombarded re TiN. The Ti 2p spectrum is formed by two contributions: an underlayer [nitride after Ar^+ bombardment shown in Fig. 2(b)] and an oxidized overlayer composed of oxynitrides. However, in the N 1s line, the oxynitride contribution is smaller than in oxidized re films without pre-bombardment [Fig. 4(b)]. The thickness of the oxidized layer is 0.97 nm versus the 2.35 nm that appears without Ar^+ pre-bombardment. As with post-bombarded as-deposited re films, the re layers are rearranged, the satellite structure essentially disappears and the films show reduced oxidation similar to the oxidation of sp films. In conclusion, a structural difference between the two kinds of nitrides, associated with the satellite structure in the Ti 2p levels, is the cause of the higher oxidation rate.

As-deposited re films were also exposed to air and the results shown in Fig. 5(b). The N 1s oxynitride contribution (shaded peak) decreases with respect to dry oxygen exposure and the Ti 2p peak of the oxidized layer shifts to higher BE (BE=457.9 eV). However, the average composition of the oxidized layer is $TiN_{0.6}$ $O_{1.25}$ with a 2.30 nm thickness. The air-exposed results indicate that re films have the same oxide layer thickness as dry oxygen-exposed re films but with higher oxygen content. The presence of a contribution at 396.1 eV in the N 1s level is a clear

indication that oxynitrides are also present in the air-oxidized layer. With this result we cannot exclude the possibility that some amount of TiO_2 is present in the surface layer.

As mentioned in the Introduction, TiN is used at SLAC as an antimultipactor secondary electron emission suppression coating on accelerator components and, for this reason, the total secondary electron emission (SEE) yield is a useful measure of the behavior of coatings exposed to air. The SEE yield (electrons out/electrons in) as a function of incident primary electron energy E_p is presented in Fig. 6 for re TiN as-deposited, oxidized, and annealed. The maximum SEE yield for as-deposited TiN is 0.93, very similar to the clean Ti metal ($\approx$ 1 [38]). Although the thickness of the dry-oxygen and air-oxidized layers is 2.3 nm, the SEE yields are very different. The maximum SEE yields are 1.10 and 1.35 for dry-oxygen and air-oxidized re TiN, respectively. The air-oxidized yield value is somewhat lower than that measured previously (1.5) in the same experimental system on air-oxidized sp TiN [12].

If either of the oxidized sp or re samples is annealed to 825 K (a typical bakeout temperature for accelerator klystron tubes), the yield drops back to below one. These results show that SEE yield of the oxide layer depends on the nature of the surface contamination, with water vapor having the strongest effect. Adsorbed water molecules create electron states which are more localized than conduction electrons in the oxide and which

resonantly capture and re-emit secondaries into vacuum [39]. After heating the adsorbed water layer is eliminated and the SEE yield decreases.

Electronic Structure

Figure 7(a) shows the XPS valence band spectra for the two types of TiN samples. The spectra have been normalized to the intensity of the corresponding Ti 3p line, so that they represent the valence-band density of states per Ti atom modulated by the respective photoionization cross sections of the levels involved. The valence band of TiN has been studied in detail. Previous experimental and theoretical data for TiN [4–10] allow one to identify the large emission band at 6 eV below the Fermi edge as due to N 2p states strongly hybridized with Ti 3d states, the so-called "p band." The structure near the edge is a nearly pure-metal Ti 3d band weakly mixed with N 2p states and is denoted as "d band."

The principal difference among the spectra shown in Fig. 7(a) lies in states close to the Fermi level, about 1.5 eV binding energy (arrow). Theoretical and experimental studies [6,8-10,40] have demonstrated that the introduction of vacancies leads to the appearance of new filled states close to 2 eV in non-stoichiometric compounds. Although the peak around 2 eV in sp TiN films could be due to vacancies, we observed the same composition in both re and sp samples, indicating that the difference between the two is due to a structural difference, which is also in agreement with the electrical conductivity differences. A similar

effect has been observed in the VO_2 valence band [41] where differences in the states close to the Fermi level are associated with conductive and nonconductive VO_2.

In a previous section, we found that the difference between re and sp samples in the Ti 2p and Ti 3p levels was in the appearance of a satellite structure shifted to higher binding energies from the principal line. Previously, Porte et al [9] found a correlation between the vacancy states at 2 eV and the satellite structure. When the number of vacancies is small the probability of core-hole screening decreases and the intensity of the unscreened final-state satellite increases. In our case, we found the same correlation between the valence band and the satellite structure, but due to structural differences rather than nitrogen vacancies. Furthermore, the reduced number of states at the Fermi level explains the poorer electrical conductivity observed in the re layer.

The valence band of re and sp TiN was also measured after Ar^+ bombardment. While in sp films, little change is observed following bombardment, new states appear around 1.5 eV in re TiN with the disappearance of the Ti 2p satellite structure.

The EELS spectra for TiN have been discussed previously in some detail [27,42–44], but confusion exists concerning losses which are due to plasmon excitations as opposed to one-electron transitions, particularly in structures at small loss energy. However, the Ti 3p and Ti 3s threshold, i.e., transitions from the Ti 3p and 3s

levels to empty Ti 3d states above Fermi level and the volume plasmon around 23 eV, are well-characterized. Figure 7(b) shows the experimental EELS spectra at a primary energy of 300 eV for the two kinds of samples at low loss energies (close to the elastic peak). The spectra show a structure at 1.7 eV and 2.7 eV for re and sp TiN, respectively. Some authors [43], studying the dielectric constant, identify the loss as a low-energy plasmon while others [27,42] choose the intraband transition dt1g—dt2g. Figure 7 shows that the energy of this structure correlates with the density of states near the Fermi edge; i.e., lower energy (1.7 eV) for re TiN in agreement with a lower density of states close to the Fermi level. After Ar^+ bombardment the density of states close to the Fermi energy increased in both kinds of samples and the peak in the EELS spectra shifted to 2.6 and 2.8 eV for sp and re TiN. Other features observed (but not shown) in the EELS spectra for both films at 23, 36, 43, and 61 eV are assigned to volume plasmons, Ti 3p–3d transition, Ti 3p resonance, and Ti 3s–3d transition, in agreement with the literature. The source of the structures around 8–12 eV is less certain.

Figure 7(a) also shows the XPS valence band spectra for as-deposited TiN before and after dry oxygen oxidation at 6.6×10^7 L exposure. The principal difference between unexposed and oxidized samples is the diminution of the "d-band" intensity close to the Fermi edge. On the other hand, comparing both oxidized spectra,

we observe more signal in the d band for the oxidized sp film, in agreement with the smaller oxide thickness. In both cases, the valence band spectra are formed by nitride and oxynitride contributions. It is interesting to observe that the diminution in the states close to the Fermi level during oxidation indicates a lower density of states close to the Fermi level for the oxynitride than for the nitride, in agreement with the more ionic character observed in the previous section.

Furthermore, the EELS spectra of both kinds of oxidized layers [Fig. 7(b)] are in agreement with the valence band results. The low energy peak closest to the elastic peak for oxidized re films appears overlapped with the elastic peak while, in sp layers, this peak appears at 2.4 eV. These results also show the correlation between this peak and the density of states close to the Fermi level.

CONCLUSIONS

Titanium nitride films of stoichiometric composition have been grown by sp and re. XPS studies of both kind of titanium nitride identify a strong satellite in re films while in sp films only a small contribution was observed. We suggest that the satellite structure is created by a structural effect that in re films produces a diminution of screening of the core hole, with a corresponding increase in the unscreened final-state satellite. The structural difference is related to increased ionicity in re TiN layer as shown in the XPS core levels and valence band.

Oxynitrides are the species that appear in the dry oxygen oxidation of both kind of layers and are characterized by the increasingly ionic character of the bonding, as shown by the XPS binding energy. Furthermore, re TiN films are more reactive to oxidation and the thickness of the oxidized layer is related to the satellite structure. On other hand, after annealing the oxidized samples at 825 K, the oxynitride disappears and a phase separation into TiN and TiO_2 is observed.

The SEE yield has been measured on as-deposited samples and after oxidation. The maximum SEE yield for as-deposited TiN is 0.93, and for annealed oxidized samples has a value lower than one. The SEE yield of the oxide layer is higher than one and depends on the nature of the surface contamination, with water vapor having the strongest effect. A low energy loss found in the EELS spectra shows a correlation with the density of states close to the Fermi level.

ACKNOWLEDGMENT

The software data acquisition and some of the curve-fitting routines used in this work were produced by Frank K. King (SLAC).

REFERENCES

[1] H.G. Tompkins, J. Appl. Phys. 70 (1991) 3876.

[2] L.E. Toth, Transition Metal Carbides and Nitrides (Academic, New York, 1971) Vol. 7.

[3] O. Knotek, M. Böhmer, and T. Leyendeker, J. Vac. Sci. Technol. A4 (1986) 2695.

[4] A. Neckel, Int. J. Quantum Chem. 23 (1983) 1317.

[5] L.I. Johansson, A. Callenas, P.M. Stefan, A. Norlund Christensen, and K. Schwarz, Phys. Rev. B24 (1981) 1883.

[6] H. Höchst and R.D. Bringans, Phys. Rev. B25 (1982) 7183.

[7] I. Johansson, P.M. Stefan, ML. Shek, and A. Norlund Christensen, Phys. Rev. B22 (1980) 1032.

[8] J. Redinger, P. Weinberger, and A. Neckel, Phys. Rev. B35 (1987) 5647.

[9] L. Porte, L. Roux, and J. Hanus, Phys. Rev. B28 (1983) 3214.

[10] P.A.P. Lindberg, L.I. Johansson, J.B. Lindström, and D.S.L Law, Phys. Rev. B36 (1987) 939.

[11] A.R. Nyaiesh, E.L. Garwin, F.K. King and R.E. Kirby, J. Vac. Sci. Technol. A4 (1986) 2356.

[12] E.L. Garwin, F.K. King, R.E. Kirby, and O. Aita, J. Appl. Phys. 61 (1987) 1145.

[13] I.R. Strydom and S. Hofmann, Vacuum 41 (1990) 1619.

[14] A. Ermolieff, P. Bernard, S. Marthon, and P. Wittmer, Surf. and Interf. Anal. 11 (1988) 563.

[15] M.J. Vasile, A.B. Emerson, and F.A. Baiocchi, J. Vac. Sci. Technol. A8 (1990) 99.

[16] B. Siemensmeyer, K. Bade, and J.W. Schultze, Ber. Bunsenges, Phys. Chem. 95 (1991) 1461.

[17] J. Halbritter, H. Leiste, H.J. Mathes, and P. Walk, Fresenius, J. Anal. Chem. 341 (1991) 320.

[18] K. S. Robinson and P.M.A. Sherwood, Surf. and Interf. Anal. 6 (1984) 261.

[19] C. Ernsberger, J. Nickerson, A.E. Miller, and J. Moulder, J. Vac. Sci. Technol. A3 (1985) 2415.

[20] C. Ernsberger, J. Nickerson, T. Smith, A.E. Miller, and D. Banks, J. Vac. Sci. Technol. A4 (1986) 2784.

[21] N.V. Hieu and D. Lichtman, Appl. Surf. Sci. 20 (1984) 186.

[22] N.C. Saha and H.G. Tompkins, J. Appl. Phys. 72 (1992) 3072.

[23] V.G. Scientific Ltd. XPS sensitivity factors for the ESCALAB MKII.

[24] P.T. Dawson and K.K. Tzatzov, Surf. Sci. 171 (1986) 239.

[25] J.E. Sundgren, B.O. Johansson, and S.E. Karlsson, Surf. Sci. 128 (1983) 265.

[26] B.J. Burrow, A.E. Morgan, and R.C. Ellwager, J. Vac. Sci. Technol. A4 (1986) 2463.

[27] L.R. Strydom and S. Hofmann, J. Electron Spec. Rel. Phenom. 56 (1991) 85.

[28] J. Pflüger, J. Fink, W. Weber, K.P. Bohnen, and G. Crecelius, Phys. Rev. B31 (1985) 1244.

[29] D.A. Shirley, Phys. Rev. B5 (1972) 4709.

[30] H.E. Bishop, Surf. and Interf. Anal. 3 (1981) 272.

[31] M. Wittmer, J. Noser and H. Melchior, J. Appl. Phys. 52 (1981) 6659.

[32] A. Ermolieff, M. Girard, C. Raoul, C. Bertrand, and T.M. Duc, Appl. Surf. Sci. 21 (1985) 65.

[33] P. Prieto, L. Galán and J.M. Sanz, Surf. and Interf. Anal. 21 (1994) 395.

[34] P. Prieto, Ph.D thesis, Universidad Autónoma de Madrid (1992).

[35] T. Chodhury, S.O. Saied, J.L. Sullivan, and A.M. Abbot, J. Phys. D 22 (1989) 1185.

[36] S. Hofmann and J.M. Sanz, J. Trace, and Microprobe Techn. 1 (1982) 213.

[37] C. Morant, L. Galán, and J.M. Sanz, Surf. Interface Anal. 16 (1990) 304.

[38] R.W. Soshea and A.J. Dekker, Phys. Rev 121 (1961) 1362.

[39] J. Halbritter, J. Appl. Phys. 53 (1982) 6475.

[40] E. Beauprez, C.H. Hague, J.M. Mariot, F. Teyssaudier, J. Redinger, P. Marksteiner, and P. Weinberger, Phys. Rev. B32 (1986) 886.

[41] D. Briggs and M.P. Seah, eds., *Practical Surface Analysis*, (John Willey and Sons, New York, 1987).

[42] B.M. Biwer and S.L. Bemasek, Surf. Sci. 167 (1986) 207.

[43] J. Plüger, J. Fink, W Weber, and K.P. Bohen, Phys. Rev. B30 (1984) 1155.

[44] W.K. Shubert, R.N. Shelton, and E.L. Wolf, Phys. Rev. B23 (1981) 5097.

FIGURE CAPTIONS

Figure 1. XPS Ti 2p and N 1s spectra of TiN (a) direct sputter-deposited and (b) reactively evaporated: experimental data (——), difference between Ti 2p of re and sp TiN (oooo), and different components (····).

Figure 2. Ti 2p and N 1s spectra of re TiN: (a) as-deposited, and after 0.5 keV Ar+ bombardment at (b) 15° and (c) 60° from the surface normal.

Figure 3. XPS spectra of sp TiN after 6.6×10^7 L dry oxygen exposure: (a) Ti 2p oxidized experimental data before (——) and after (- - -) subtraction of the clean sp TiN spectrum; (b) component fit of the oxidized data; (c) component fit of N 1s oxidized data into nitride (····) and oxynitride (shaded area).

Figure 4. Ti 2p, N 1s, and O1s spectra of re TiN: (a) as-deposited, (b) following 6.6×10^7 L dry oxygen exposure, and (c) after heating to 825 K in UHV for 8 hours. experimental data (——), Ti 2p after subtraction of the clean re TiN spectrum (- - -), fitting components (····), and oxynitride (shaded area).

Figure 5. Ti 2p and N 1s spectra of (a) air-exposed re TiN and (b) 0.5 keV Ar+ ion bombarded and oxidized re TiN, 6.6×10^7 L dry oxygen exposure: experimental data (——), Ti 2p after subtraction of the clean re TiN spectrum (- - -), fitting components (····), and oxynitride (shaded area).

Figure 6. Total secondary electron emission yield coefficient (electrons out/electrons in) for re TiN (a) as-deposited, (b) after 6.6×10^7 L dry oxygen exposure, (c) as-deposited and air-exposed and (d) samples (b) or (c) after heating to 825 K.

Figure 7. (a) Mg K_α-excited valence bands of re and sp TiN after 6.6×10^7 L dry oxygen exposure, and (b) the correspond-ing EELS spectra in the low energy loss region. The low energy loss peaks of interest are marked by dashed lines (- - -). The arrow at 1.5 eV in the valence band marks the position of structure-induced filled states near the Fermi

Table I. TiN Binding Energies

Parameter	TiN (sp)	TiN (re)
E_b (Ti $2p_{3/2}$)	454.70	455.10
ΔE_b (metal)	0.70	1.10
E_b (N 1s)	397.10	396.90
FWHM (N 1s)	1.20	1.65
ΔE (satellite)	- - -	1.70
E_b (Ti $2p_{3/2}$–N1s)	57.60	58.20
After Dry Oxygen Oxidation		
E_b (Ti $2p_{3/2}$)	455.50 457.70	457.05
E_b (N 1s)	396.10	395.90
E_b (O1s)	531.70	531.20
ΔE (Ti $2p_{3/2}$–O1s)	74.00–76.20	74.15

Energy error $\approx$ 0.05 eV, E_b (Ti $2p_{3/2}$, metal) = 454.00 eV, and E_b (Ti $2p_{3/2}$, TiO_2) = 458.90 eV

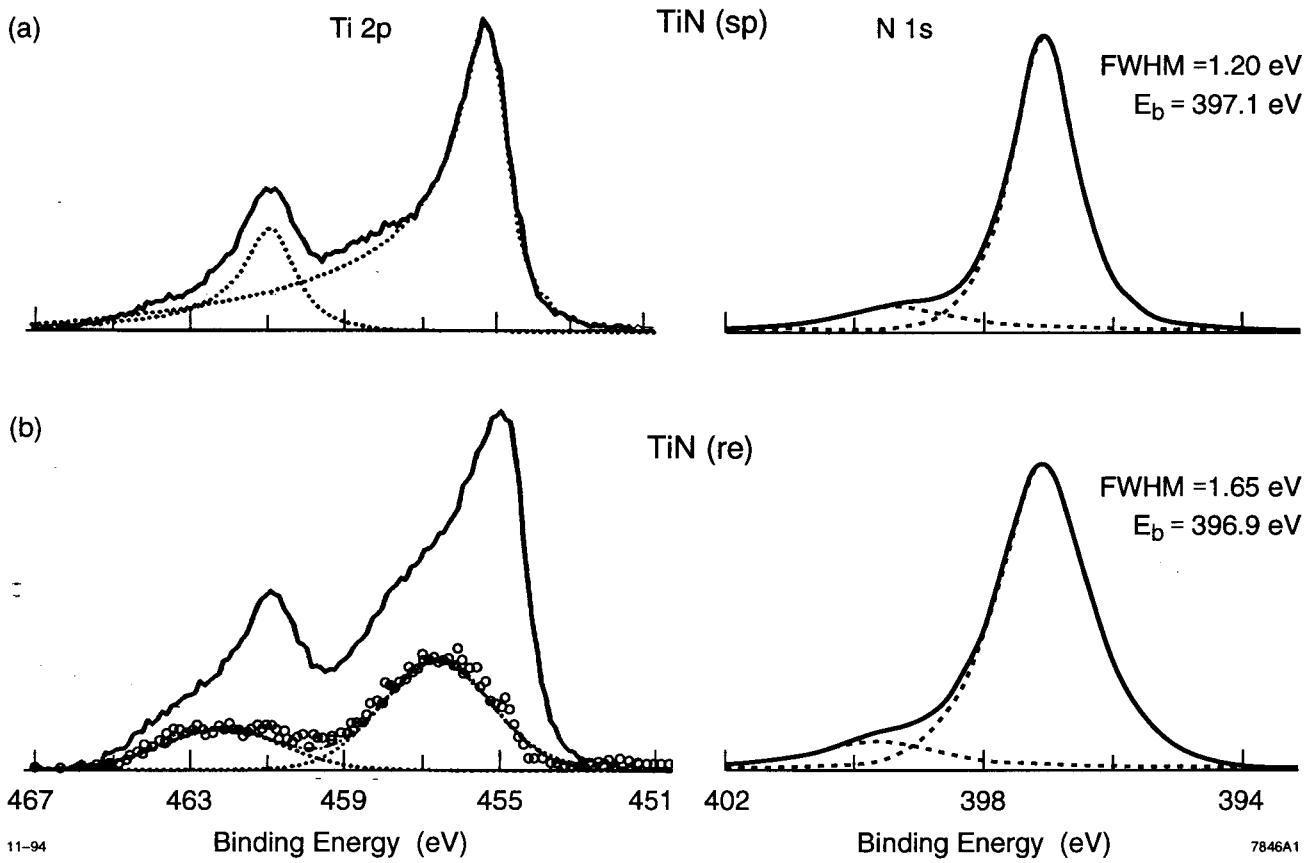
(a)
Ti 2p
TiN (sp)
N 1s
FWHM =1.20 eV
E_b = 397.1 eV
(b)
TiN (re)
FWHM =1.65 eV
E_b = 396.9 eV
467
463
459
455
451
402
398
394
11-94
Binding Energy (eV)
Binding Energy (eV)
7846A1

Fig. 1

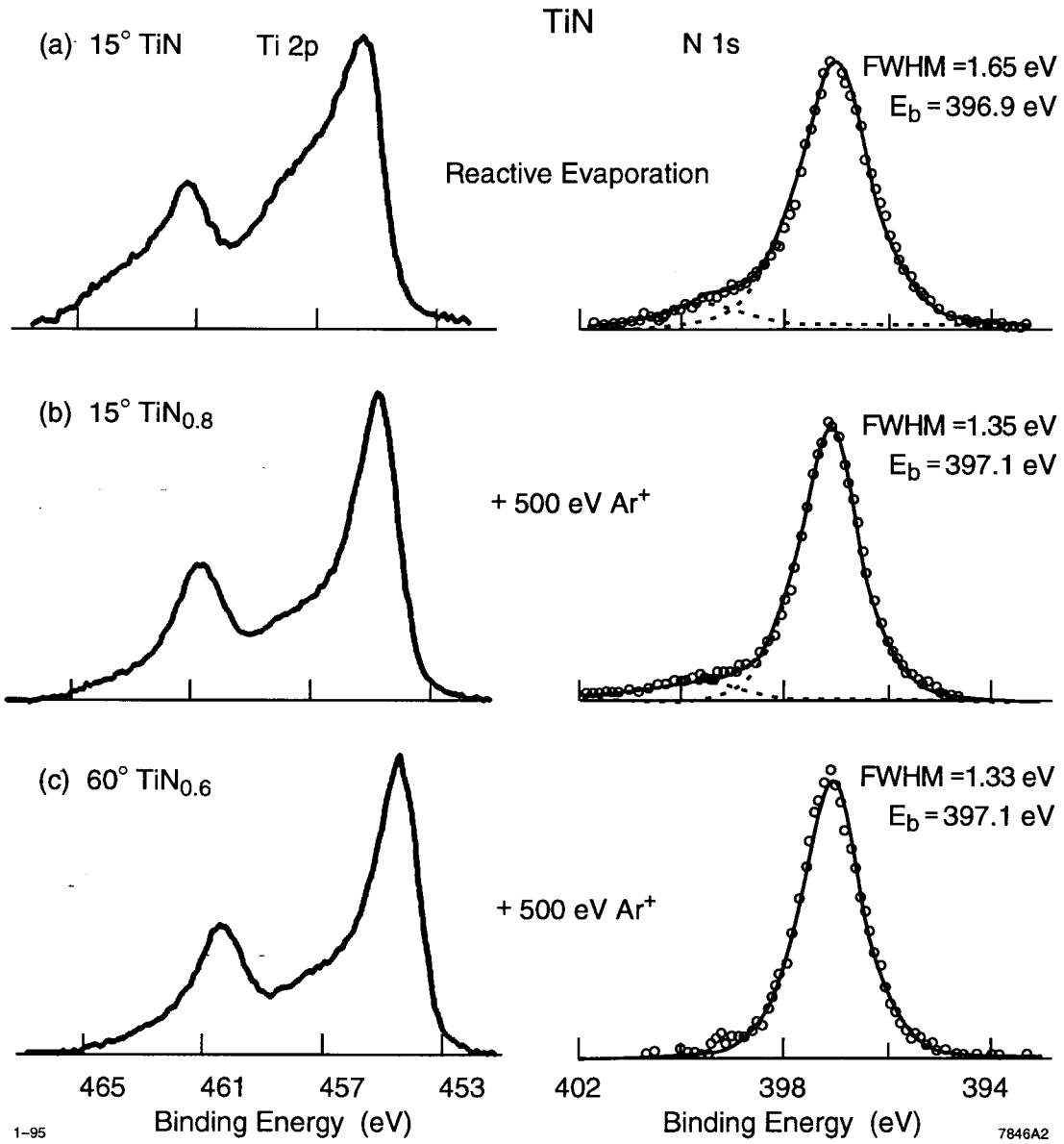
TiN
(a) 15° TiN
Ti 2p
N 1s
FWHM =1.65 eV
E_b = 396.9 eV
Reactive Evaporation
(b) 15° $TiN_{0.8}$
FWHM =1.35 eV
E_b = 397.1 eV
+ 500 eV Ar^+
(c) 60° $TiN_{0.6}$
FWHM =1.33 eV
E_b = 397.1 eV
+ 500 eV Ar^+
465
461
457
453
Binding Energy (eV)
402
398
394
Binding Energy (eV)
1-95
7846A2

Fig. 2

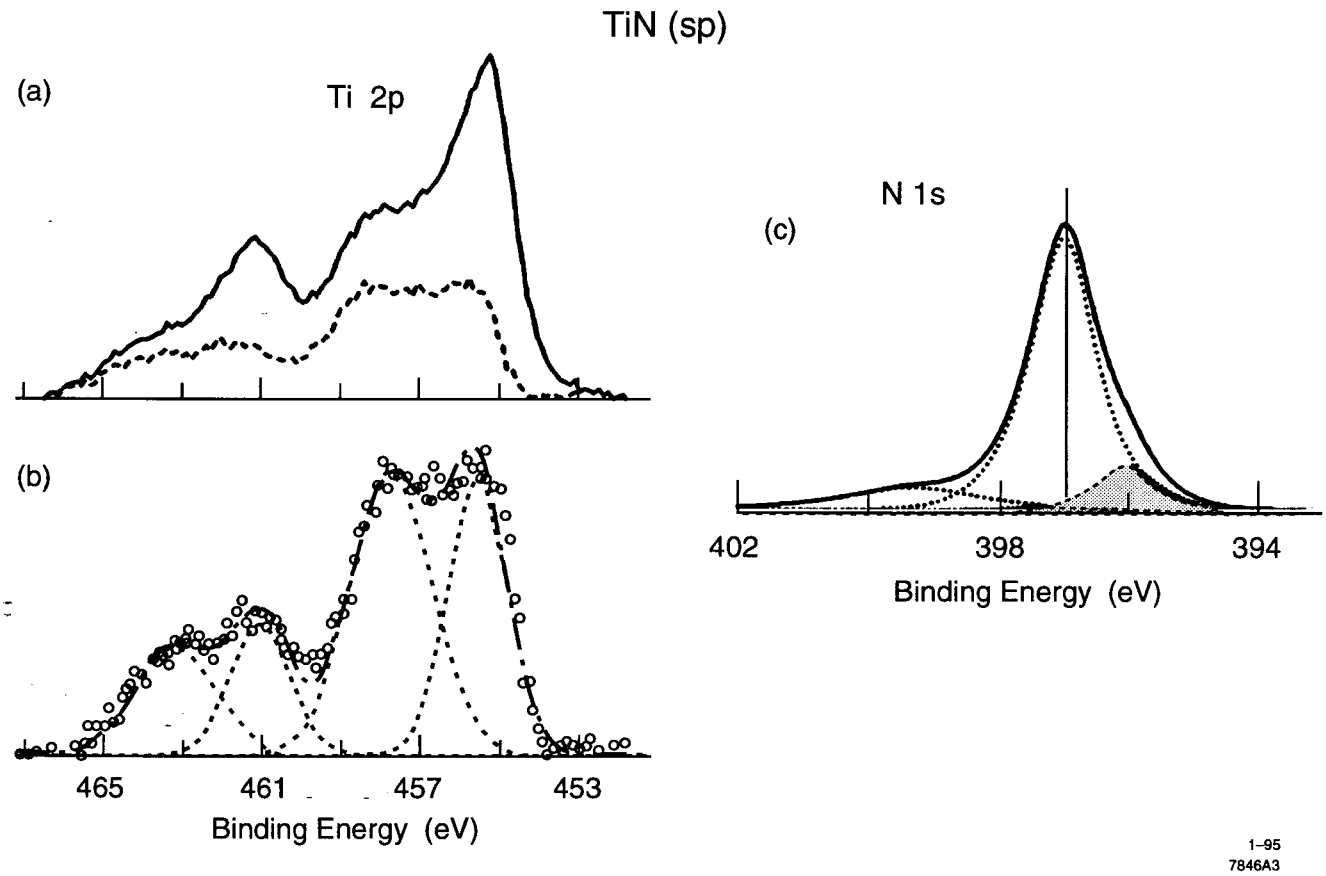
TiN (sp)
(a)
Ti 2p
(b)
465
461
457
453
Binding Energy (eV)
(c)
N 1s
402
398
394
Binding Energy (eV)
1–95
7846A3

Fig. 3

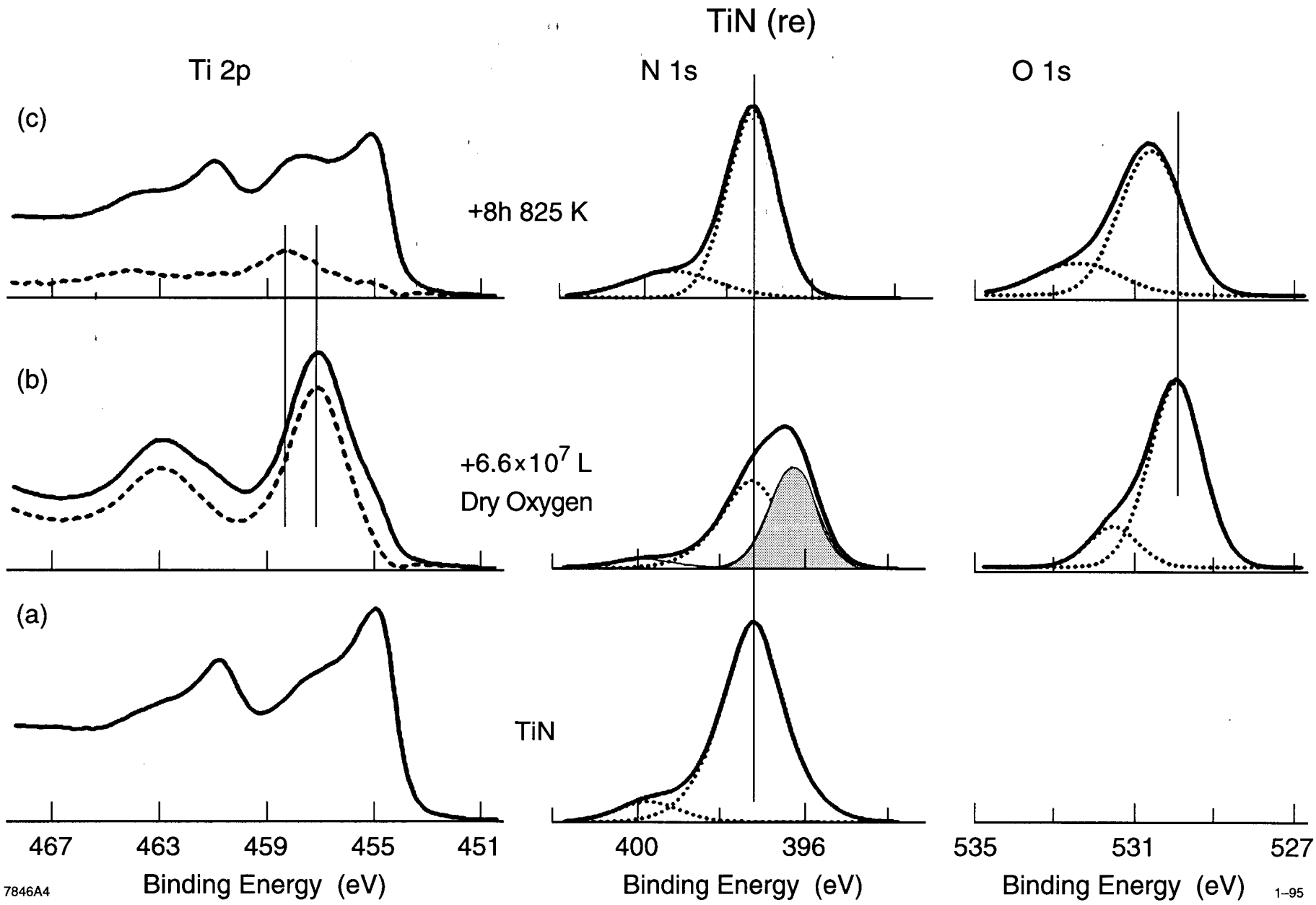
TiN (re)
Ti 2p
N 1s
O 1s
(c)
+8h 825 K
(b)
+6.6×10^7 L
Dry Oxygen
(a)
TiN
467
463
459
455
451
400
396
535
531
527
Binding Energy (eV)
Binding Energy (eV)
Binding Energy (eV)
7846A4
1–95

Fig. 4

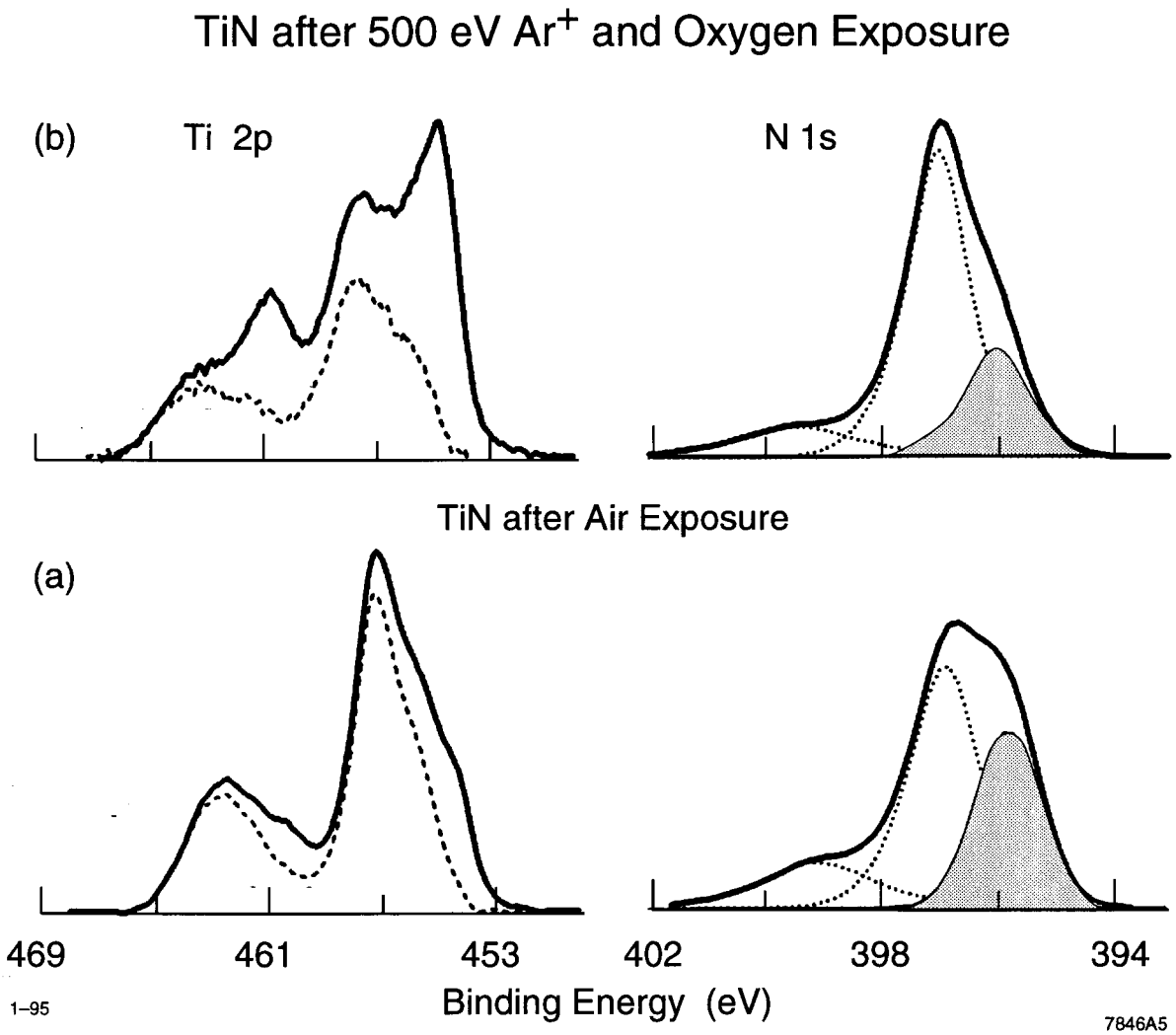
TiN after 500 eV Ar+ and Oxygen Exposure
(b)
Ti 2p
N 1s
TiN after Air Exposure
(a)
469
461
453
402
398
394
Binding Energy (eV)
1–95
7846A5

Fig. 5

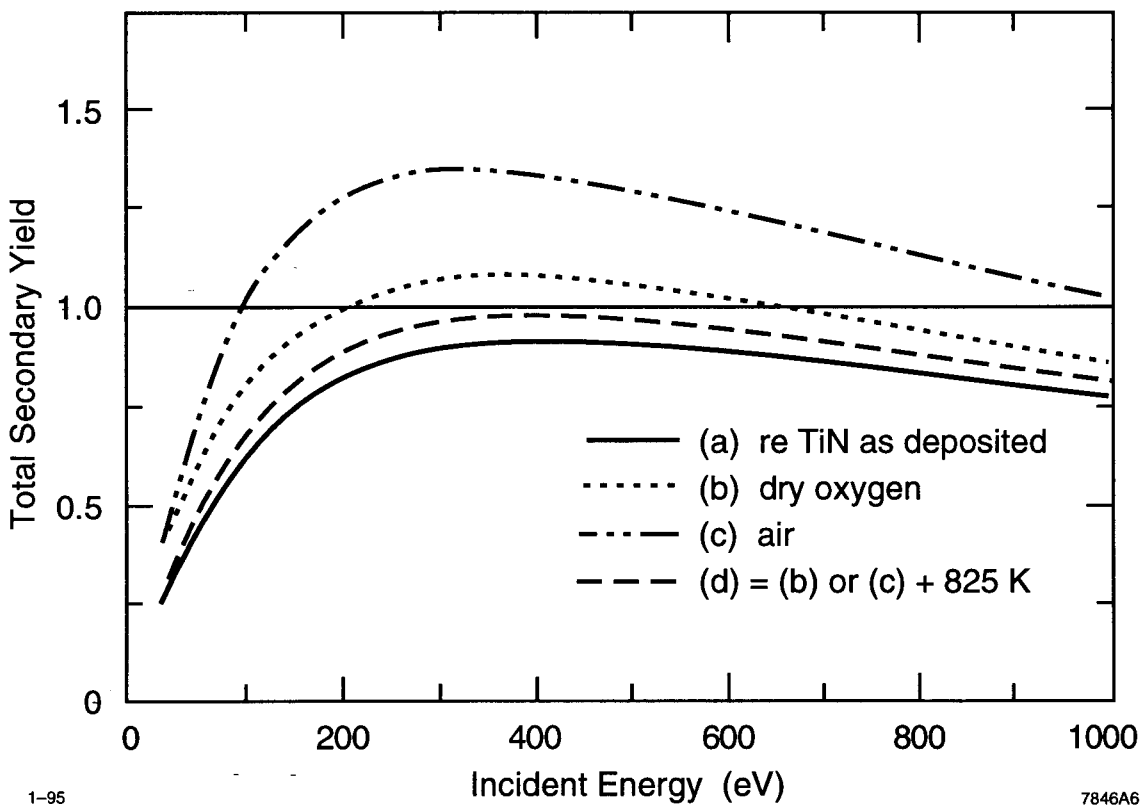
1.5
1.0
0.5
0
Total Secondary Yield
0
200
400
600
800
1000
Incident Energy (eV)
(a) re TiN as deposited
(b) dry oxygen
(c) air
(d) = (b) or (c) + 825 K
1–95
7846A6

Fig. 6

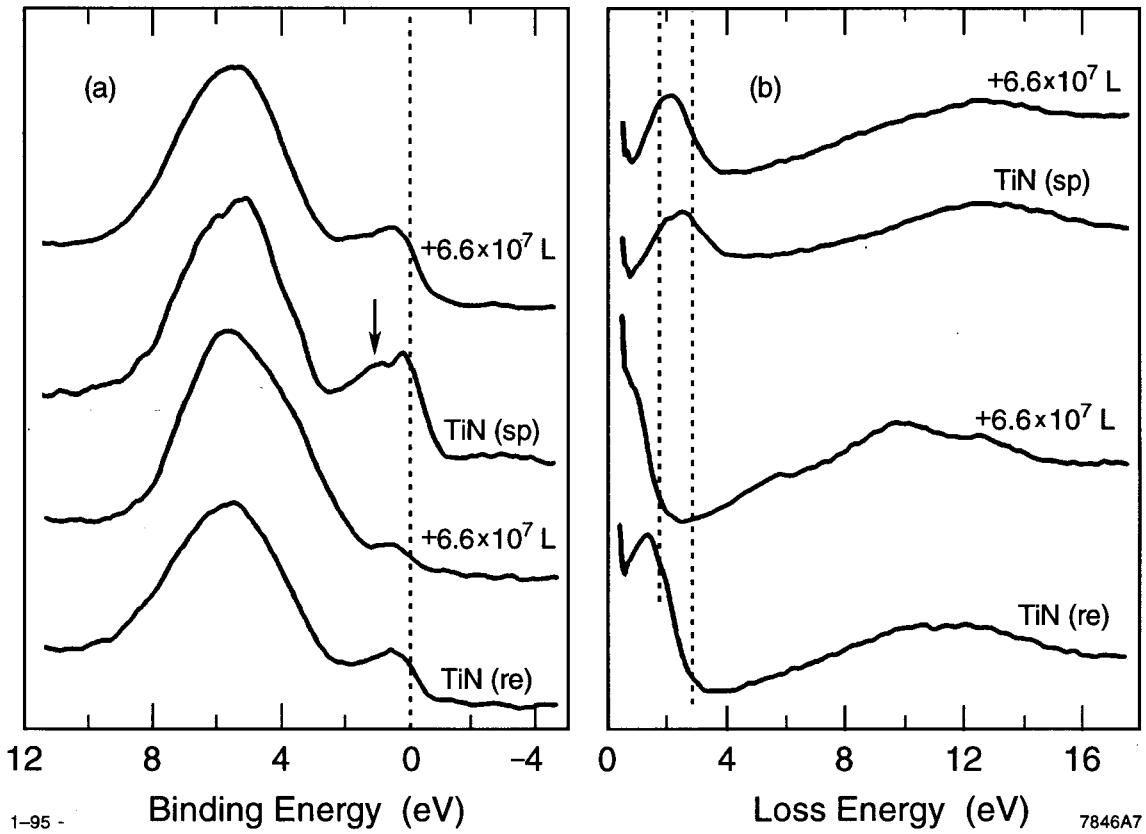
(a)
+6.6x10^7 L
TiN (sp)
+6.6x10^7 L
TiN (re)
12
8
4
0
-4
Binding Energy (eV)
(b)
+6.6x10^7 L
TiN (sp)
+6.6x10^7 L
TiN (re)
0
4
8
12
16
Loss Energy (eV)
1-95
7846A7

Fig. 7